Green public procurement applied to partially precast reinforced concete slabs

Engineering Structures 301 (2024) 117338

Contents lists available at ScienceDirect

Engineering Structures

journal homepage: www.elsevier.com/locate/engstruct

Green public procurement applied to partially precast reinforced concete slabs

Alessandro P. Fantilli

Dept. of Structural, Building and Geotechnical Engineering - DISEG, Politecnico di Torino, Corso Duca degli Abruzzi 24, 10129 Torino, Italy

ARTICLE INFO

Keywords:
Concrete with recycled materials
Predalles
Three-point bending tests
Eco-mechanical analysis
Three-stage model

ABSTRACT

To build environmentally friendly public constructions, authorities impose tailoring concrete mixtures with a minimum content of recycled materials. To satisfy this green public procurement (GPP) in frame structures, whose mass is mainly distributed on horizontal diaphragms, it is necessary to draw attention to the slabs of floors. As ready-mixed concrete with recycled materials is not easily available on the market, partially prefabricated one-way slabs, composed by both cast-in-situ concrete and precast plates (generally called predalles) were investigated. Only the precast concrete of predalles contained recycled materials, such as supplementary cementitious materials (SCM) in place of CEM I, recycled concrete aggregate (RCA) and rubber to replace stone aggregate, and recycled steel fibers (RSF). These materials were used to cast full-scale one-way slabs, subsequentially tested in three-point bending. A three-stage model, based on the equivalence between the traditional rebar and RSF, was also introduced to predict the load-deflection responses of the slabs. As results, both numerical and experimental analyses revealed the effectiveness of RSF, which can be added to concrete mixtures to compensate the loss of flexural strength that the substitution of virgin materials produces. Thus, if large quantities of SCM, RCA, rubber, and RSF are in the concrete of predalles, slab can satisfy both GPP and the mechanical performances, though the cast-in-situ concrete does not contain any recycled material.

1. Introduction

The environmental impact of structural concrete is mainly due to the large use of cement, whose production, based on the cooking of limestone and clay at 1500 °C, releases in the atmosphere about 8–9% of the global anthropogenic CO_2 [1]. On the other hand, the demand for sand and gravel, which are the largest part by mass of a concrete mixtures [2], is rising faster than the natural renewal [3]. Thus, to reduce the impact of concrete, the so-called substitution strategy must be applied by replacing cement and aggregates with recycled materials [4].

For instance, supplementary cementitious materials (SCM) can be a valid environmental-friendly alternative to Portland cement [5]. They are either byproducts or waste materials (such as fly ash), to be used in blended cements, or as additive in concrete mixtures. In the same way, natural aggregates can be substituted by recycled concrete aggregate (RCA) coming from construction and demolition waste [6], and by rubber from end-of-life tires [7]. Although the latter produces a weaker concrete [8], several advantages arise when scarp or crumb rubbers are used to substitute the traditional stone aggregate. Indeed, rubberized concrete under uniaxial compression expands significantly and, in the presence of an FRP-confinement, a lateral prestress can be generated. Therefore, the strength and the stiffness of concrete columns significantly increase [9]. In addition, the bond between steel rebar and concrete improves in presence of rubber aggregate [10]. Tires also offer other materials to concrete industry, such as polymeric fibers [11] and recycled steel fibers (RSF) [12], which can substitute the reinforcing bars of concrete structures.

Research activities on the substitution strategy can be used to fulfil public requirements. Indeed, public investments on works, goods, and services (including concrete, which is the most consumed manufactured material in the world by mass [1]) represent a large part of the gross domestic products of several countries (e.g., it is about 14% in Europe) [13]. Accordingly, by means of the so-called Green Public Procurement (GPP), each member state of the EU introduced rules to procure concrete with a reduced environmental impact. For instance, in Italy, concrete used in public constructions must contain at least 5% by mass of recycled materials [14].

This prescriptive approach seems not appropriate for the current (and future) building codes, which are mainly performance-based. However, according to Bigaj-van Vliet et al. [15], prescriptive

E-mail address: alessandro.fantilli@polito.it.

https://doi.org/10.1016/j.engstruct.2023.117338
Received 23 August 2023; Received in revised form 5 November 2023; Accepted 11 December 2023
Available online 20 December 2023

approaches are the easiest way to foster the use of recycled materials, regardless of the real impact on sustainability. This is due to the lack of general approaches capable of linking the properties of recycled materials of a mixture and the mechanical performances of concrete structures. In other words, although the substitution strategy was largely applied in the past, and several models capable of predicting the behavior of reinforced concrete structures were proposed as well, they were not used to design and produce reinforced concrete (RC) structures in accordance with also GPP. As a matter of fact, Fennel et al. [16] predicted that it will take more than a decade to effectively satisfy the sustainability requirements (i.e., the current GPP), which are some of the evolving needs of structural engineering.

With the aim of shortening the time and promoting the application of GPP within the concrete industry, new sustainable one-way slabs are investigated herein. They generally form the horizontal diaphragms of buildings, where most of the concrete mass is present. Hence, in the following sections, after tailoring and testing new concrete mixtures (Section 2), the results of a wide experimental campaign are illustrated (Section 3) and rated by means of the eco-mechanical model (Section 4). Finally, a refined mechanical model is also introduced to predict the structural behavior of full-scale one-way slabs containing recycled materials (Section 5).

2. The production of concrete slabs according to GPP

Fig. 1a shows a predalle, which is an RC panel having a thickness of 50 mm, a width of 1200 mm, and a length L equal to floor span. Through the addition of cast-in-situ concrete, predalle can be used to build a floor slab, whose cross-section is illustrated in Fig. 1b. To resist permanent and live loads acting on the floor, predalle is generally reinforced with steel rebars in x and y directions. Moreover, to facilitate the handling, resist the temporary loads [17], and to improve the bond between precast and cast-in-situ concrete, streel trusses are also introduced (see Fig. 1a). As the amount of longitudinal rebars is generally close to the minimum reinforcement ratio (rather than to the maximum) recommended by code rules, it can be furtherly reduced when steel fibers are added to concrete mixtures [18]. Finally, when predalles are used for public constructions and produced by an Italian precast plant, the concrete panel must contain at least 5% by mass of recycled materials [13, 14].

2.1. Concrete mixtures for predalles

The concrete mixture of current predalles, herein considered as reference and called Ref., is only made with virgin materials. It is composed by three fractions (0–4 mm, 0–8 mm, and 4–14 mm) of virgin stone aggregates, Portland cement (CEM I 52.5 R), tap water, and an acrylic superplasticizer. The mass of each component, referred to 1 cubic

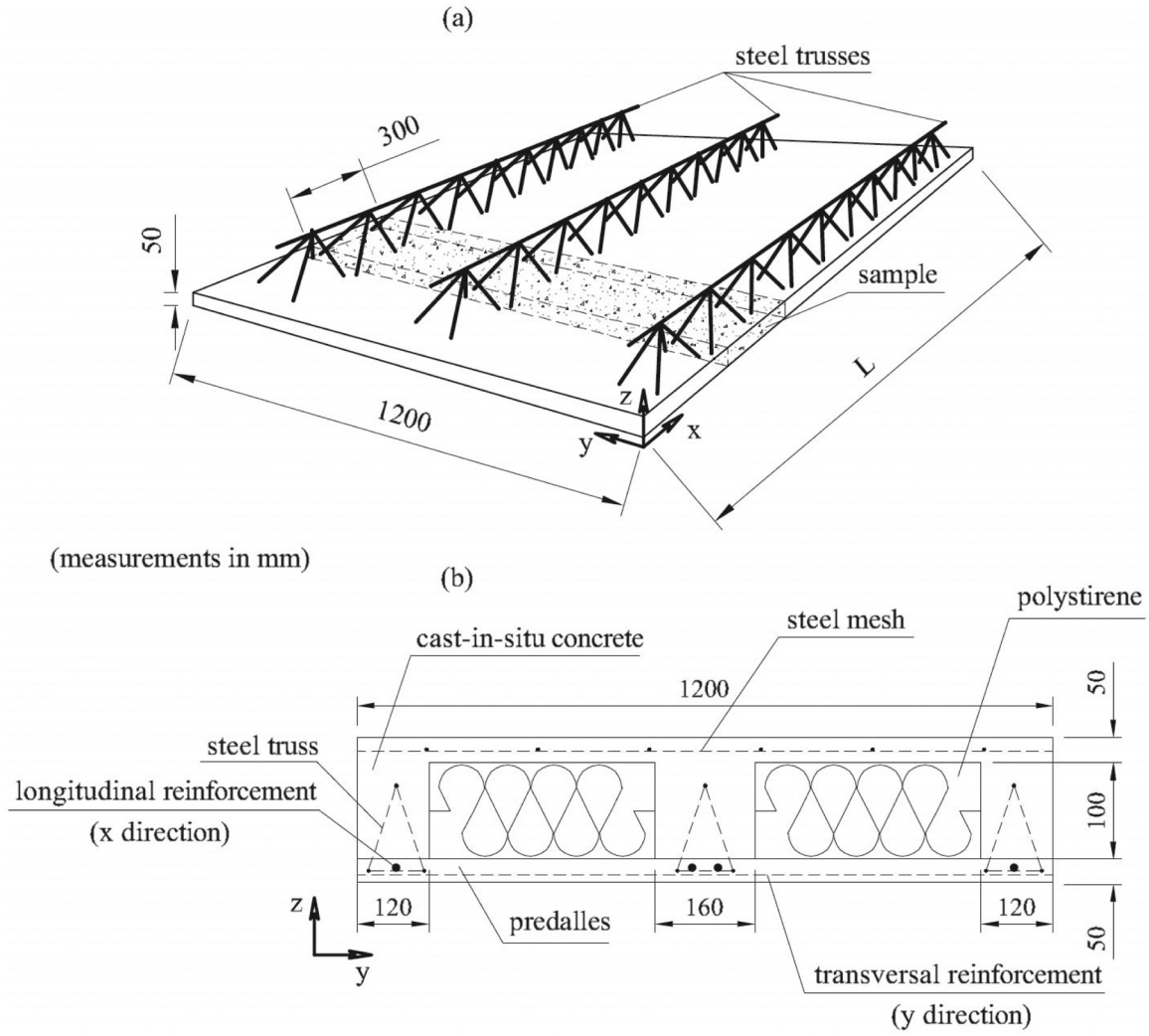

Fig. 1. – Partially precast slab of floors: (a) precast predalle; (b) typical cross-section of a slab.

meter of concrete, is reported in Table 1. In addition to Ref., other four mixtures (named A, B, C, and D) were tailored by using 20% of CEM I 52.5 R and 80% of CEM III 42.5 N (which contained 40% of SCM) as binder.

In the concrete type A, aggregate fractions are the same as Ref., whereas 48 kg/m^3 (about 0.5% in volume) of RSF from end-of-life tires were added (see Fig. 2). These fibers had an average length of 15.8 mm, a diameter of 0.62 mm, and an average aspect ratio of 62.8 [19]. As the water-to-binder ratio remained unchanged, the content of super-plasticizer increased to maintain the same workability of concrete Ref. In this way, in concrete type A the percentage of recycled materials, computed as the ratio between the sum of the masses of recycled components and the sum of the masses of all the components, was $R = 8\%$.

The value of R increased and reached 40% in concrete type B, where the aggregate fraction 6–15 mm of concrete type A and Ref. was entirely replaced by RCA, having the same size. With respect to concrete type A, in concrete type C only 160 kg of virgin stone aggregate 0–8 mm was substituted with the same size and volume of rubber from end-of-life tires. For this concrete, $R = 11\%$. Finally, in concrete type D, it was possible to reach $R = 45\%$, because both the whole aggregate fraction of 6–15 mm and 160 kg of the fraction 0–8 mm, contained in the concrete type A and Ref., were substituted by RCA and by the same size and volume of rubber from end-of-life tires, respectively.

2.2. Material properties

With the four mixtures A, B, C, and D reported in Table 1, it was possible to tailor fiber-reinforced concrete (FRC), capable of fulfilling GPP in Italy (where $R \geq 5\%$), and cast five full-scale predalles (width = 1.2 m, thickness = 5 cm, and length $L = 5$ m). As shown in the last column of Table 1, a number from 1 to 5 was associated to each predalle, depending on the type of concrete mixture. To characterize these concretes, a total of 15 cylinders (3 per each mixture) were also cast and tested in uniaxial compression. As shown in Fig. 3a, they had a height of 300 mm and a diameter of 150 mm.

Instead of the prism 150 × 150 × 600 mm^3, on which the mechanical properties of the fiber-reinforced concrete are generally measured [20,21], the sample illustrated in Fig. 1a was tested in bending (Fig. 3b-c). Indeed, this sample allowed a FRC characterization closer to the real conditions, because it had a thickness (of 50 mm) and a length (of 1200 mm) equal, respectively, to the thickness and the width of the real predalles [22].

For the new sample, a width of 300 mm (Fig. 3b) was selected in order to have a deflection-softening behavior in sample 1 [23], made with concrete Ref. and reinforced with a single rebar of diameter $\Phi = 5$ mm (see Fig. 3c). The same test was performed on samples 0, 2, 3, 4, and 5, having the same geometry of Fig. 3b, but made with the concretes Ref., A, B, C and D, respectively (see the second last column of Table 1), without any rebar. For these samples, a deflection softening behavior was also expected.

In each test, carried out at Politecnico di Torino (Italy), every single sample was supported by two steel cylinders, whereas a third cylinder, in contact with a loading cell (whose stroke moved at a velocity of 0.2 mm/min), was used to apply the load P in the mid-section (Fig. 3a). In addition, 4 LVDTs (with a maximum elongation of ± 25 mm) measured the displacements in four different points (2 in the midspan and 1 on each support). By means of these measurements, the midspan deflections η were computed and associated to the applied load P up to the complete failure of the specimens.

Fig. 2. Recycled steel fibers (RSF) from end-of-life tires.

2.3. Tests on full-scale slabs

With the above-mentioned predalles, 5 one-way slabs were cast and numbered as in the last column of Table 1. The cross-section of the slab, as depicted in Fig. 1b, was composed by the precast panel of predalle (the bottom flange), and by a cast-in-situ concrete of the upper flange and by the three longitudinal joists [24]. The total depth was 200 mm, whereas the width coincided with that of the predalle. From a practical point of view, it can be modelled as I-shaped cross-section (Fig. 4a), in which the width of the central web is the sum of the widths of the three joists (120 + 160 + 120 mm).

There were 3 levels of longitudinal reinforcement (i.e., in the x direction of Fig. 1b) in each slab: 4 rebars with a diameter $\Phi = 10$ mm and 6 rebars of $\Phi = 5$ mm (included in the trusses of predalles) were in the bottom flange; 3 rebars of $\Phi = 7$ mm (included in the trusses of predalles) reinforced the web; and a mesh of $\Phi = 5$ mm at 200 mm (i.e., 6 rebars of $\Phi = 5$ in Fig. 4a) was placed in the upper flange. In addition, a transversal reinforcement (i.e., in the y direction of Fig. 1b), composed by 1 rebar of $\Phi = 5$ mm every 300 mm, was only present in the bottom flange of slab 1. In the other slabs (i.e., slab 2, slab 3, slab 4, and slab 5) made with FRC predalles (i.e., with the concrete mixtures A, B, C, and D)

Table 1
Composition (per cubic meter) of the concrete mixtures used in the predalles of partially precast slabs.

Type of concrete mixture	CEM III 42.5 R	CEM I 52.5 R	Fractions of virgin aggregates			Water	Fractions of Recycled aggregates		RSF	Superplasticizer.	R	Sample number	Slab and predalle number
			(0-2 mm)	(0-8 mm)	(6-15 mm)		Rubber (0-8 mm)	RCA (6-15 mm)					
	(kg)	(kg)	(kg)	(kg)	(kg)	(kg)	(kg)	(kg)	(kg)	(l)	(%)		
Ref.	0	384	360	816	728	165	0	0	0	2.6	0	0 (plain) 1 (RC)	1
A	307	77	360	816	728	165	0	0	48	3.5	8	2	2
B	307	77	360	816	0	165	0	728	48	4.2	40	3	3
C	307	77	360	656	728	165	43	0	48	3.5	11	4	4
D	307	77	360	656	0	165	43.2	728	48	4.2	45	5	5

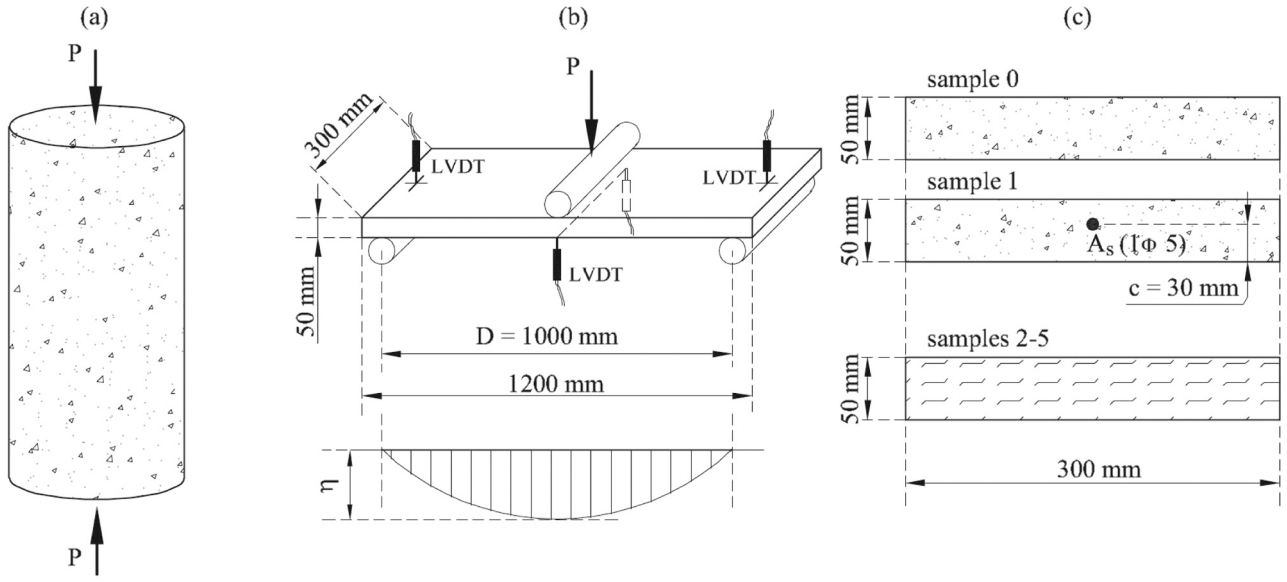

Fig. 3. Measuring the material properties: (a) cylinders for uniaxial compression tests; (b) tree point bending test in a sample extracted from predalles; and (c) possible cross-sections of the samples.

the transversal reinforcement was substituted by RSF. As these fibers also offered a contribution to the longitudinal reinforcement, in the I-shaped cross-section of Fig. 4a an additional level of reinforcing bar is present in the bottom flange. This extra-reinforcement, equivalent to FRC [22], consisted of 1 rebar of $\Phi = 5$ mm every 300 mm of the flange width.

The slabs were tested in three-point bending on a span $L_1 = 4.5$ m (see Fig. 4b). Namely, each slab was supported by two steel cylinders, whereas a third cylinder, in contact with a loading cell (whose stroke moved at a velocity of 0.8 mm/min), was used to apply the load F in the mid-section. In addition, 6 potentiometric transducers (with a maximum elongation of $\pm$ 100 mm) measured the displacements in six different points (2 in the midspan and 2 on each support). These measurements were used to compute the midspan deflection δ associated to the load F.

3. Test results

3.1. Material properties

Table 2 shows the values of the compressive strength measured by testing in uniaxial compression the 15 cylinders (Fig. 3a) cast with the concretes listed in Table 1. The results of other two tests, performed on the cast-in-situ concrete of the slabs, are also reported in the last two rows of Table 2.

Concerning the flexural behavior of the samples depicted in Fig. 1a and Fig. 3b-c, the load-midspan deflection (P-η) curves are drawn in Fig. 5 (the number of the samples are those already reported in Table 1). In each diagram, the thicker curve represents the average behavior measured on 6 samples of the same type.

In the case of sample 0 (Fig. 5a), the maximum load (or the failure load) varied from 2.46 kN to 2.98 kN, with an average value of 2.69 kN. As soon as this peak was reached, the sample failed in a brittle manner (i.e., in the presence of a single crack), without any residual strength in the post-cracking stage. Indeed, for $\eta \geq 2$ mm (i.e., at 1/500 of the sample span), the concrete cross-section showed no strength, and $P = 0$ (i.e., the bridging effect in the cracked cross-section vanished).

In sample 1 (see Fig. 5b), the maximum load was within the range 2.31 $\sim$ 2.74 kN, with an average value of 2.47 kN. After reaching the peak load, the failure of the sample occurred in the presence of a single crack. Moreover, the yield strain of the steel rebar occurred at a load P lower than that of cracking (the typical brittle failure of under-reinforced concrete samples). Nevertheless, due to the bridging effect of the rebar across the crack, a residual strength (i.e., $P > 0$) was observed. More precisely, when the rebar yielded at $\eta = 3.87$ mm, the value of P was constant and equal to 0.76 kN.

In samples containing recycled fibers and aggregates (i.e., from sample 2 to sample 5), the mechanical response in bending depended on the type and the amount of recycled materials. In particular, the average value of the maximum load varied from 2.04 kN of concrete type A (sample 2) to 1.65 kN of concrete type B (sample 3).

Although all these samples failed in a brittle manner (i.e., with a single crack), residual strengths were clearly visible in the post cracking stage, because of the bridging capacity of the fibers. In particular, when $\eta = 3.87$ mm (i.e., when the rebar of $\Phi = 5$ mm yielded in the sample 1) the average residual load P was about 0.73 kN (the same of sample 1) in all the FRC elements (from sample 2 to sample 5), regardless of the type and the amount of recycled (nonfibrous) materials within the concrete mixtures (see Fig. 5c-f).

3.2. Three-point bending tests on full-scale slabs

The load-deflection (F-δ) diagrams of the 4 slabs made with predalles containing recycled materials (i.e., slabs 2–5 in Table 1) are illustrated in Fig. 6. These F-δ curves are compared with that of slab 1, whose predalle was composed by only virgin materials.

The best performances of slab 2, having predalle reinforced by both rebar and RSF of concrete type A, is evident (Fig. 6a). More precisely, in service, when $\delta/L_1 = 1/250$ (i.e., $\delta = 18$ mm), and at ultimate limit state, when $\delta/L_1 = 1/125$ (i.e., $\delta = 36$ mm), slab 2 showed values of the applied loads F higher than those of slab 1, despite the same content of reinforcing bars (Fig5a).

Nevertheless, when the virgin stone aggregate of predalles was substituted by either RCA (slab 3 in Fig. 6b), or rubber (slab 4 in Fig. 6c), the differences with respect to slab 1 vanished. Indeed, at the two values of deflection ($\delta = 18$ mm, and $\delta = 36$ mm), the loads F measured in slab 2 and slab 3 were almost coincident with those of slab 1.

Conversely, in the case of slab 5 (Fig. 5d), whose predalle was made with concrete type D (i.e., with rubber and RCA in substitution of virgin stone aggregate), the values of F were lower than those of slab 1 for all the deflections.

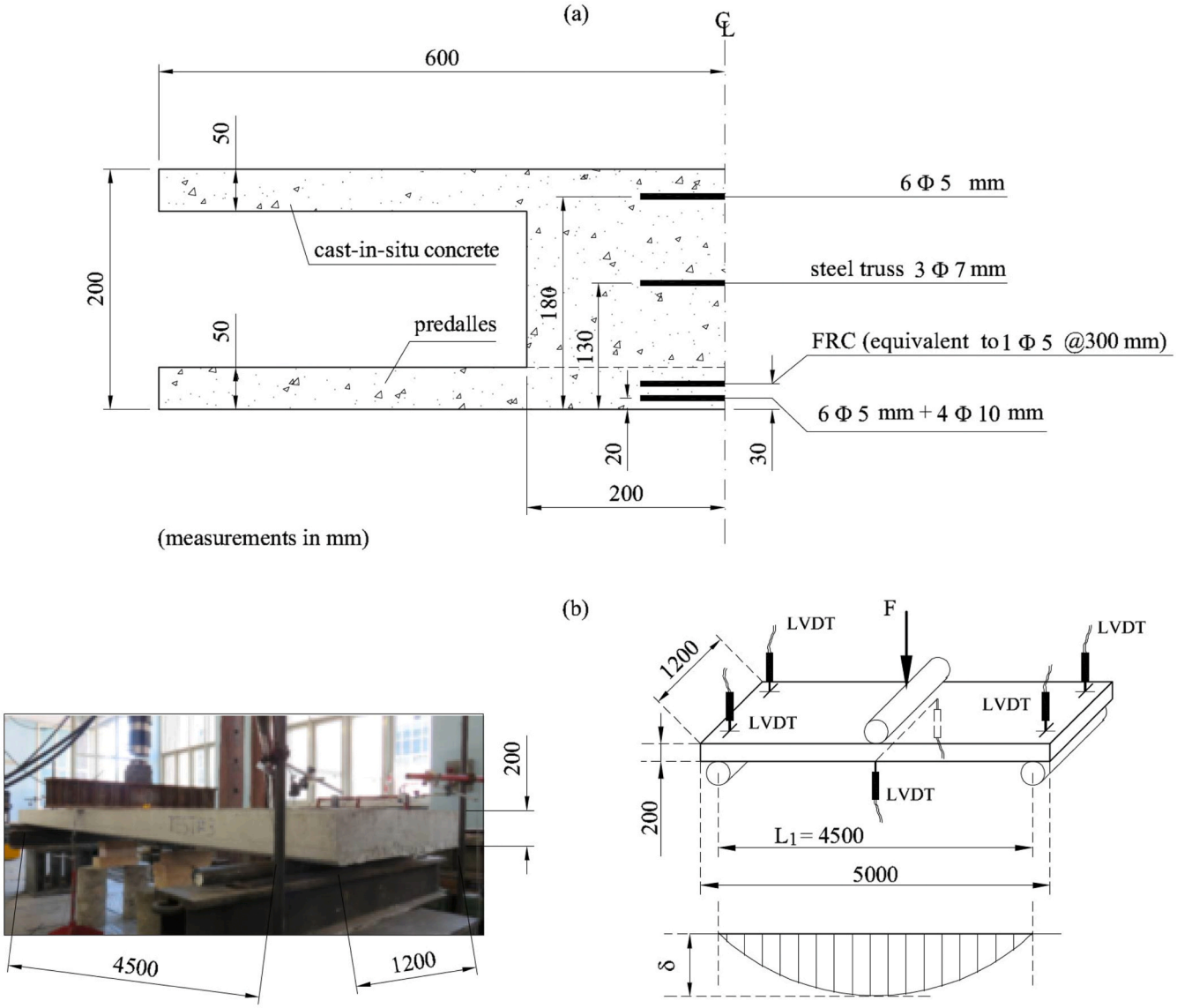

Fig. 4. Full-scale partially precast slabs: (a) I-shaped cross-sections with the longitudinal reinforcements; (b) static configuration of the three-point bending tests.

Table 2
Results of the uniaxial compression tests on concrete cylinders.

Type of concrete mixture	Mass	Average Diameter	Average Height	Area of cross-section	Density	Load at failure	f_c Compressive strength
	(kg)	(mm)	(mm)	(mm^3)	(kg/m^3)	(kN)	(MPa)
Ref.	12.5	153	290	18441	2331	878	47.6
	12.5	153	289	18463	2337	874	47.4
	12.5	149	291	17541	2437	802	45.7
A	12.4	153	290	18330	2333	705	38.4
	12.4	153	290	18293	2325	689	37.7
	12.3	152	288	18218	2345	692	38.0
B	11.2	153	290	18292	2119	391	21.4
	11.1	153	292	18338	2070	402	21.9
	11.9	154	293	18669	2179	447	24.0
C	11.5	153	287	18335	2197	411	22.4
	11.4	153	285	18368	2166	392	21.3
	11.4	153	285	18316	2182	394	21.5
D	10.1	152	284	18231	1951	302	16.5
	10.4	153	288	18296	1979	293	16.0
	10.4	153	286	18333	1984	307	16.8
Cast in situ	12.4	152	294	18199	2325	903	49.6
	12.5	153	294	18308	2316	920	50.2

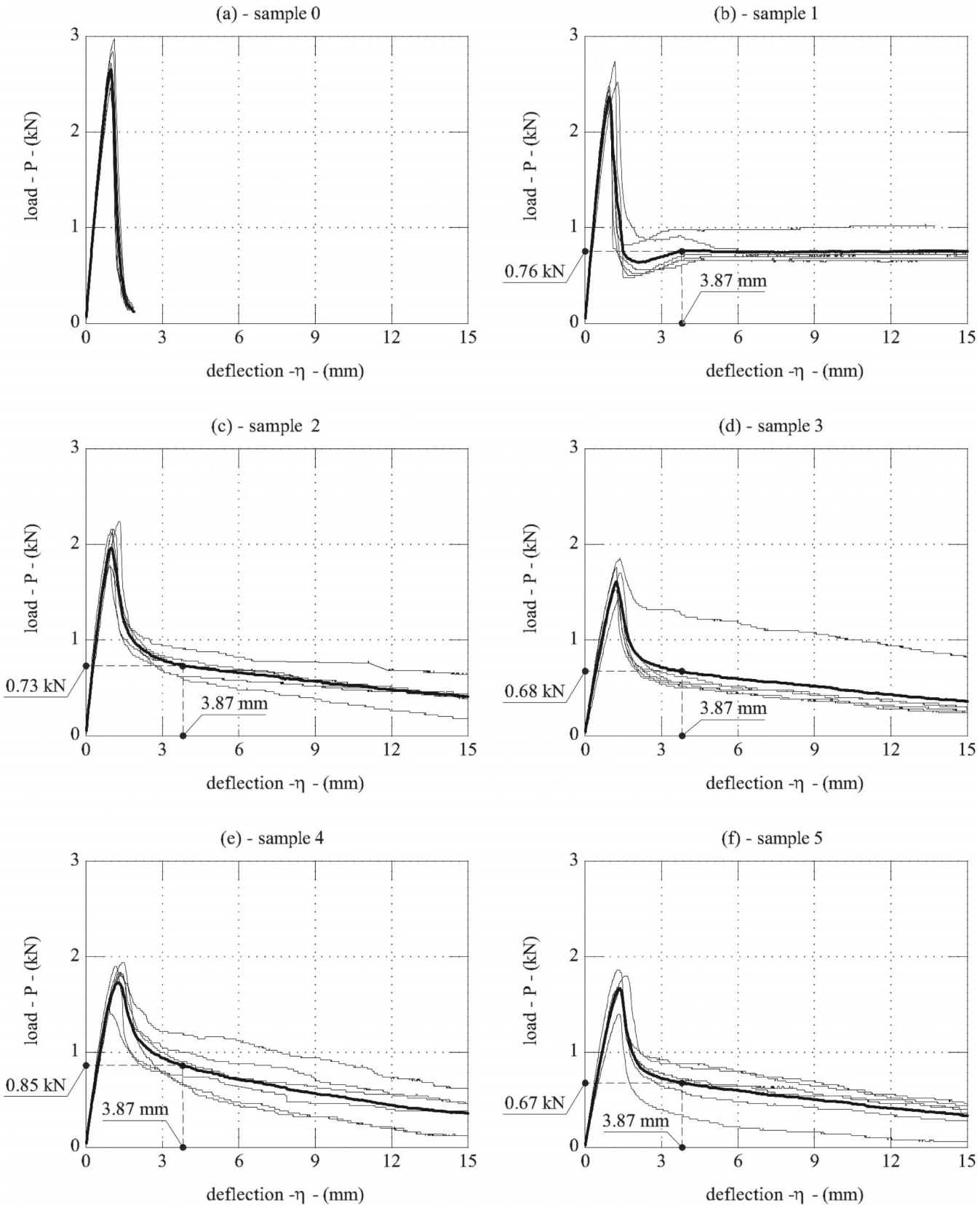

Fig. 5. Load-midspan deflection *P*-η curves measured through the flexural tests on samples of predalles.

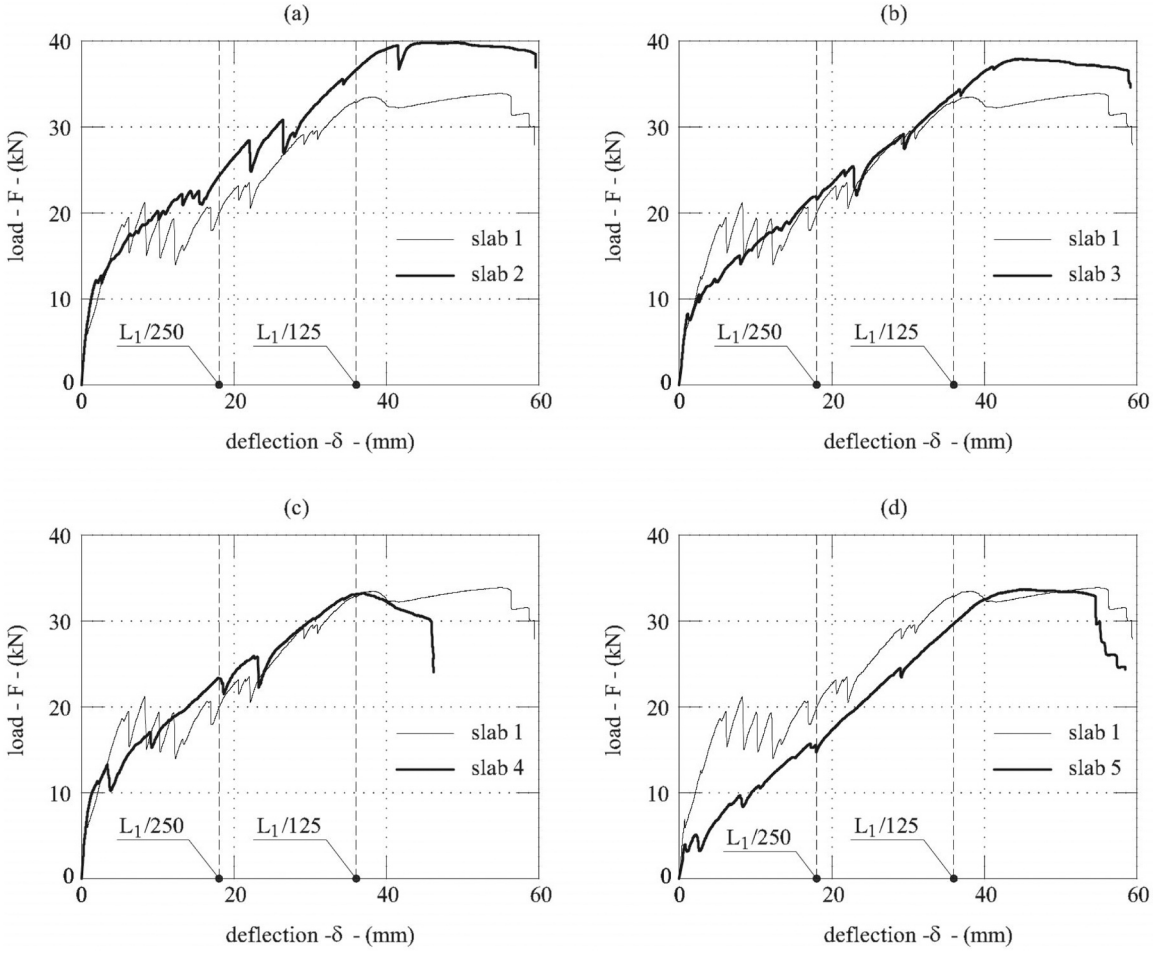

Fig. 6. Comparing the load midspan deflection *F*-δ curves of the slab 1, containing only virgin materials, with those of the other slabs made with recycled materials.

4. Eco-mechanical analysis of results

According to Fantilli and Nishiwaki [25], the mechanical and environmental performances of materials and structures have to be rated by means of eco-mechanical charts, like those illustrated in Fig. 7. In these charts, the mechanical index, reported on the abscissa MI ($= f / f_{min}$), represents the ratio between the measured mechanical performance f (which is a sort of functional unit) and the minimum value f_{min} fixed by tenders and building codes.

Similarly, the ordinate shows the values of ecological index EI ($= R / R_{min,GPP}$), which is the ratio between the environmental performance of concrete (herein assumed to be the percentage of recycled materials R) and the minimum prescribed by green public procurement, $R_{min,GPP}$. In some European Countries, the construction market does not offer a large volume of cast-in-situ concrete with RCA (in Italy is only 0.4% [26]), thus R (and EI) are herein referred to only the concrete in the precast slab of predalles. Accordingly, the lines EI = 1 (minimum ecological performance, corresponding to $R = R_{min,GPP}$) and MI = 1 (minimum mechanical performance, corresponding to $f = f_{min}$) divide the eco-mechanical charts of Fig. 7 into 4 sectors. When the performances are defined by the points that fall within the top right sector (where EI > 1 and MI > 1), concretes can be accepted from both environmental and mechanical point of view.

Referring to the Italian GPP, which impose $R_{min,GPP} = 5\%$, and to the case of $f = f_c$ = average compressive strength of concrete (i.e., the average values of f_c experimentally measured and reported Table 2) and f_{min} = 28 MPa (e.g., the average strength of the minimum class of structural concrete suggested by Eurocode 2 [27]), the eco-mechanical chart depicted in Fig. 7a reveals that only concrete type A can be accepted. Concrete Ref. showed the best mechanical performance (MI ≅ 2) but, being made without any recycled material (i.e., $R = 0$), it cannot satisfy GPP. On the contrary, concretes type B, C and D, with a percentage of recycled materials $R > 5\%$ (and EI > 1), can satisfy GPP, even if MI < 1, because the compressive strengths are lower than f_{min} (see Fig. 7a). This behavior has been largely reviewed in the technical literature, as the substitution of virgin materials with those recycled, especially rubber, leads to a loss of compressive strength [6–8].

Nevertheless, the result of the eco-mechanical analysis differs by changing the functional unit f. In particular, by moving from compressive strength to the flexural strength, it is possible to maintain the same values of EI (the GPP prescription is the same) and consider $f = P$ when η = 3.87 mm (see Fig. 5). Hence, if f_{min} = 0.76 kN (i.e., that of sample 1, made with concrete Ref. and 1 rebar of Φ = 5 mm), both sample 2 with concrete type A and sample 4 with concrete type C fall within the top right sector (see Fig7b). Conversely, sample 3 and sample 5, made with concrete type B and type D, respectively, can only satisfy the GPP requirement.

To sum up, concrete type A (sample 2) performs better both in compression and in bending, even if the residual flexural strength of sample 4, made by concrete type C, is the highest. In other words, although the compressive strength of concrete tends to reduce in presence of rubber, the latter can guarantee a remarkable contribution in flexure after cracking [28].

If the structural behavior of the slabs in service is taken into consideration, the eco-mechanical analysis can be performed by assuming the same EI previously introduced at material level, whereas f

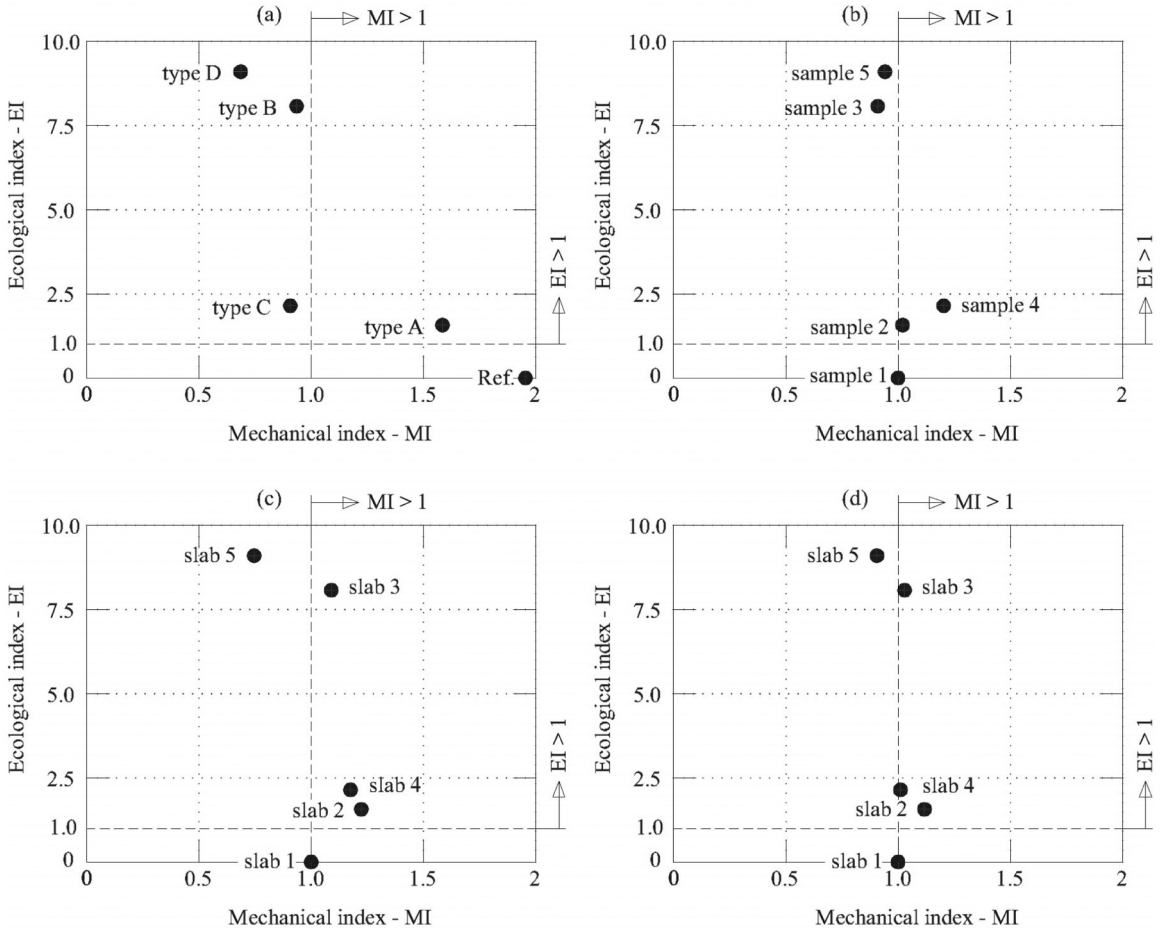

Fig. 7. Eco-mechanical analysis of test results: (a) on concrete cylinders when $f = f_c$; (b) on predalle samples when $f = P$ at $\eta = 3.87$ mm; (c) on slabs when $f = F$ at $\delta = 18$ mm; and (d) on slabs when $f = F$ at $\delta = 36$ mm.

$= F$ when $\delta/L_1 = 1/250$ can be used to compute MI. In this case, f_{min} is that of slab 1, with the predalle currently produced. The results shown in Fig. 7c reveal the good performances of slabs 2, 3, and 4, which satisfy not only GPP but also the mechanical performances. This is due to the contribution of RSF, which is weak when it is measured on the samples (see Fig. 5c-f), but it becomes significant when the predalles are in the bottom of the slab cross-section illustrated in Fig. 1b. Nevertheless, this benefic contribution is not sufficient in the predalle with concrete type D (i.e., slab 5), where the loss of mechanical performance due to the presence of SCM, RCA, and rubber is not compensated by the structural contribution given by the recycled steel fibers.

As these observations are also true at the ultimate limit state, when $f = F$ at $\delta / L_1 = 1/125$ (see Fig. 7d), an effective application of GPP can be argued from the eco-mechanical analyses of the full-scale slabs. Indeed, the structural response of slab 3, whose predalle was cast with concrete type B, is practically similar to that of slab 1 (see Fig. 6b, Fig. 7c, and Fig. 7d) containing only virgin materials. As predalles constituted 37.5% of the cross-section depicted in Fig. 1b, the whole slab 3 can satisfy GPP. Indeed, the total percentage of recycled material in this slab is 15% (i.e., the product of 37.5% times $R = 40\%$ of concrete type B), although the cast-in-situ concrete contained only virgin materials. Considering that in some European Countries a small percentage of RCA is currently added to cast-in-situ concrete [26], and that the major part of the mass of buildings is concentrated into the rigid horizontal diaphragms [29], GPP will be satisfied by an entire RC structure if predalles with concrete type B is used to cast the slabs of floors.

Finally, comparing the results of Fig. 7c and Fig. 7d with those of Fig. 7b, it clearly appears the necessity of modifying code rules, which require a minimum compressive strength also when concrete is only subjected to tensile stresses. This is the case of predalle, whose concrete is only located in the tensile zone of the simply supported slab depicted in Fig. 4. As shown in Fig. 6b, when type B concrete (with an average compressive strength of 22.4 MPa) is in the tensile zone of slab 3, the P-δ response does not differ from that the reference slab 1, in which the average compressive strength of predalle is 46.9 MPa (i.e., that of concrete type A). Therefore, to foster the application of recycled materials, the required minimum strength has to be related to the use of concrete containing these materials.

5. Modelling the behavior of slabs with predalles

When a prescriptive approach is adopted, like that of GPP, it is necessary to assess whether structures containing recycled materials can guarantee minimum mechanical performance, or not. In the previous sections, the suitability of partially precast slabs with predalle was checked with a full-scale experimental campaign (Fig. 4). However, these tests are expensive and time consuming, therefore models capable of predicting the F-δ curves shown in Fig. 6 are needed.

As the input data should include the properties of non-conventional concrete mixtures (type A, B, C, and D in Table 1), a refinement of the three-stage model developed for concrete beams reinforced with rebar and fibers [30] is proposed herein for one-way slabs with predalles. In particular, the first stage remarkably differs from that proposed by Fantilli et al. [30], because the presence of all the recycled materials is taken into account with an equivalent steel rebar. In the second and third stages, moment-curvature relationships are calculated and used to

compute the possible range of *F*-δ.

5.1. Stage 1 - The effect of reinforcement

The samples shown in Fig. 3b-c can be used to evaluate the resisting contribution P_{reinf} of either rebar or fibers. As suggested by Falkner and Henke [31], it is:

$$P_{reinf} = P - P_{plain} \quad (1)$$

where P = total load measured in the RC or FRC sample; and P_{plain} = total load measured in an unreinforced sample (i.e., sample 0). Fig. 8 shows the P_{reinf} – η and P – η curves of sample 1 (Fig. 8a) and sample 2 (Fig. 8b), made with concrete Ref. reinforced with 1 rebar of Φ = 5 mm and concrete type A, respectively.

When η < 1 mm, P_{reinf} is practically zero, or even negative, regardless of the type of reinforcement. Thus, the resisting contribution of the samples can be mainly ascribed to the cementitious matrix. When concrete cracks, at η ≥ 1 mm, P_{reinf} becomes greater than 0. In the case of RC samples (sample 1 in Fig. 8a), P_{reinf} increases, but when η ≥ 3.87 mm (at which steel rebar yields) it remains constant. Nevertheless, the values of P coincide with those of P_{reinf}, starting from lower values of deflections. In other words, when the resisting contribution of the matrix in tension vanishes (at η ≅ 1.9 mm) only the reinforcement provides a resistance contribution to tensile actions. Thus, in these under-reinforced concrete samples, the fracture mechanism of concrete can be neglected (i.e., $P = P_{reinf}$) also before the yielding of the rebar [30].

In the sample 2 made with type A concrete (Fig. 8b), and in all the other FRC samples, due to the presence of recycled steel fibers, P_{reinf} rapidly grows for η ≥ 1 mm, but it subsequently reduces. The decrement of the mechanical response is due to the pullout of the fibers, which provided the only resisting mechanism in the tensile zone of the cracked cross-section in bending. Indeed, also for these samples, P coincides with P_{reinf} when η ≥ 1.9 mm.

In general, it is possible to assume that when η ≥ 3.87 mm (i.e., at ultimate limit state of sample 1), P_{reinf} decreases linearly with η in the samples reinforced with fibers, and the following general equation can be introduced:

$$P_{reinf} = P_0 + \alpha \quad \eta \quad (2)$$

where the coefficients P_0 and α can be calculated from a linear regression of the experimental data, when η ≥ 3.87 mm. Table 3 shows the values of P_0 and α for all the samples, whereas the lines of Eq.(2) are reported in Fig. 8a for sample 1 and in Fig. 8b for sample 2.

In the case of sample 1, it is possible to correlate the σ − ε constitutive law of the steel rebar A_s (1 rebar of Φ = 5 mm) with the curve P_{reinf} - η (see Fig. 9). When $\eta = \eta_2$, steel rebar yields (i.e., $\varepsilon = \varepsilon_{sy}$) and, for $\eta > \eta_2$, both P_{reinf} and the stress of steel σ remain constant. In the case of $\eta_1 < \eta < \eta_2$, the strain of rebar is in the linear elastic regime (with $0 < \varepsilon < \varepsilon_{sy}$), therefore P_{reinf} (Fig. 9a) and σ (Fig. 9b) show monotonic increments.

For the other samples (i.e., from sample 2 to sample 5) with recycled

Table 3
Parameters of the equivalent flexural behavior of samples made with different concretes.

Sample number-type of concrete	P_0 (kN)	α (kN/mm)	σ_1 (MPa)	σ_2 (MPa)	β (MPa)
1 – RC	0.75	0.0006	–	–	–
2 – type A	0.83	-0.0288	587.8	567.4	23360
3 – type B	0.76	-0.0275	539.2	519.7	22300
4 – type C	0.99	-0.0440	692.4	661.3	35690
5 – type D	0.77	-0.0299	547.4	526.3	24250

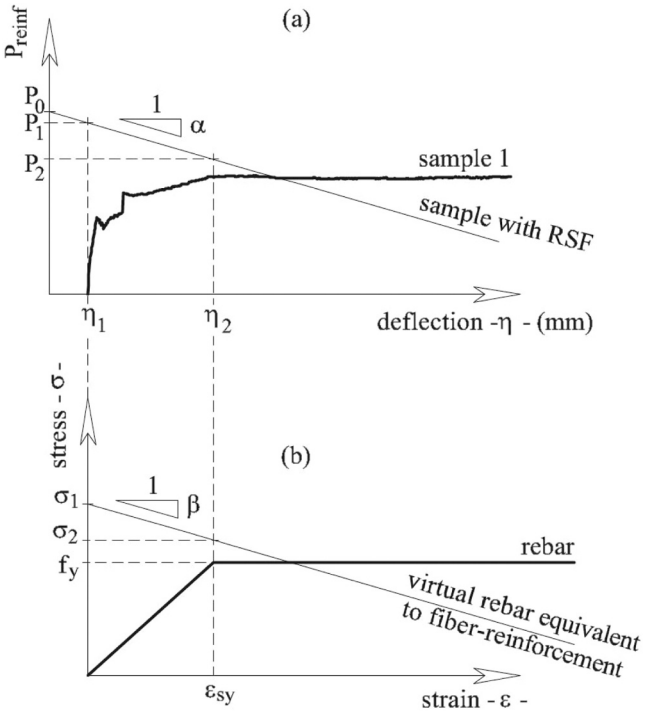

Fig. 9. Correlation between steel reinforcing bar of sample 1 and the fiber-reinforcement of samples 2–5: (a) *P*-η response of the samples; (b) stress-strain relationship of rebar and equivalent rebar.

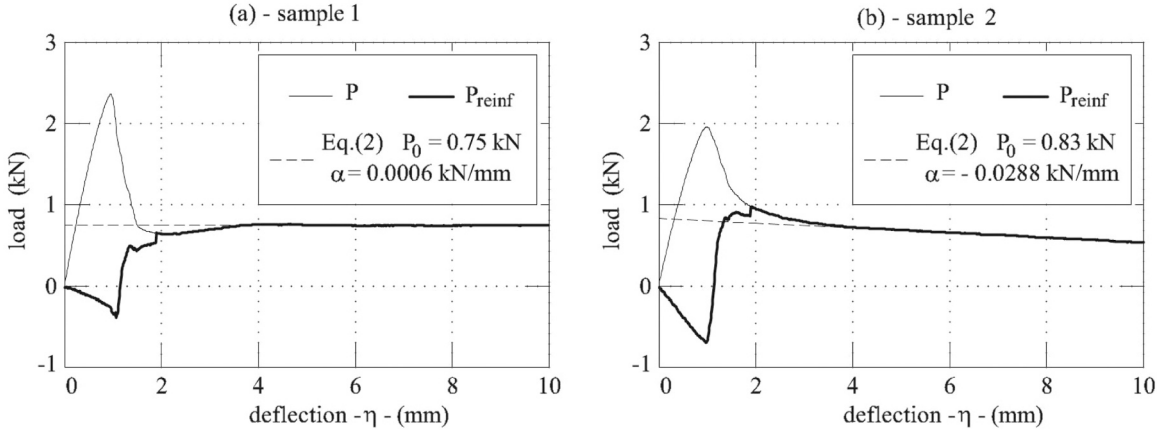

Fig. 8. Resisting contribution of the reinforcement in (a) sample 1, reinforced with a single steel rebar (Φ = 5 mm); and in (b) sample 2, reinforced with RSF.

fibers and aggregates, a linear decrement of P_{reinf} with the deflection $\eta > \eta_1$ can be conjectured, as α of Eq.(2) is lower than zero (see Table 3). If P_{reinf} was provided by an equivalent rebar A_s (with $\Phi = 5$ mm), the constitutive relationship of this virtual rebar would not be elastic-perfectly plastic, but it would decrease linearly with ε (see Fig. 9b):

$$\sigma = \sigma_1 - \beta \quad \varepsilon \tag{3}$$

where: $\beta = \frac{\sigma_1 - \sigma_2}{\varepsilon_{sy}} \sigma_i = \frac{P_{reinf}}{4} \frac{D}{0.9d} \bullet \frac{1}{A_s}$ (with i = 1 or i = 2).

D = span length of the sample (= 1000 mm in Fig. 3b); d = effective depth of the cross-section in sample 1 (= 20 mm in Fig. 3c); and ε_{sy} = strain at yielding of steel rebar. The values of σ_1, σ_2, and β of the FRC samples listed in Table 3 can be used to define the mechanical properties of the single rebar ($\Phi = 5$ mm every 300 mm) equivalent to FRC.

5.2. Stage 2 The moment-curvature relationship

To compute the moment-curvature (M-χ) relationships of the I-shaped cross-section depicted in Fig. 4a, the mechanical properties of materials must be defined in advance. For the constitutive law of the steel rebar, the bilinear stress-strain (σ-ε) relationship of Fig. 10a is assumed. The parameters of this relationship were experimentally measured through uniaxial tensile tests. The ascending branch of the Sargin's parabola [20] is the σ-ε law of compressed concrete in the slab cross-section (Fig. 1b). As it is mainly composed by the cast-in-situ concrete of the upper flange and of the three joists, the average compressive strengths reported in the last two rows of Table 2 are used to define the parameter of $\sigma - \varepsilon\square$.

On the contrary, the uncracked stage of the concrete in tension, composed by the predalles, is reproduced by a linear $\sigma - \varepsilon$ relationship. Both the elastic modulus E_c and the tensile strength f_{ct} are evaluated in accordance with Model Code 2010 [20], starting from the value of concrete strength f_c experimentally measured and reported in Table 2. As the softening stage of this concrete exists only in presence of fibers, it is modelled by assuming an equivalent rebar $\Phi = 5$ mm every 300 mm (see Fig. 4a), having the constitutive relationship defined in the previous section.

According to Fantilli et al. [30], to include the tension-stiffening contribution within the M-χ relationship, the situations of incipient cracking (maximum tension stiffening) and fully cracked behavior (minimum tension-stiffening) must be considered. For the sake of the simplicity, the maximum tension-stiffening is supposed to occur when the concrete of predalles shows a pseudo-plastic behavior in tension, regardless of crack width. Thus, referring to the equivalent rebar behavior shown in Fig. 9, it is assumed that $\sigma = \sigma_1$ for all the values of ε. Similarly, for the minimum tension-stiffening, it is possible to neglect the resisting contribution of the equivalent rebar, and $\sigma = 0$ for all the ε. Accordingly, two M-χ curves are computed, like those illustrated in

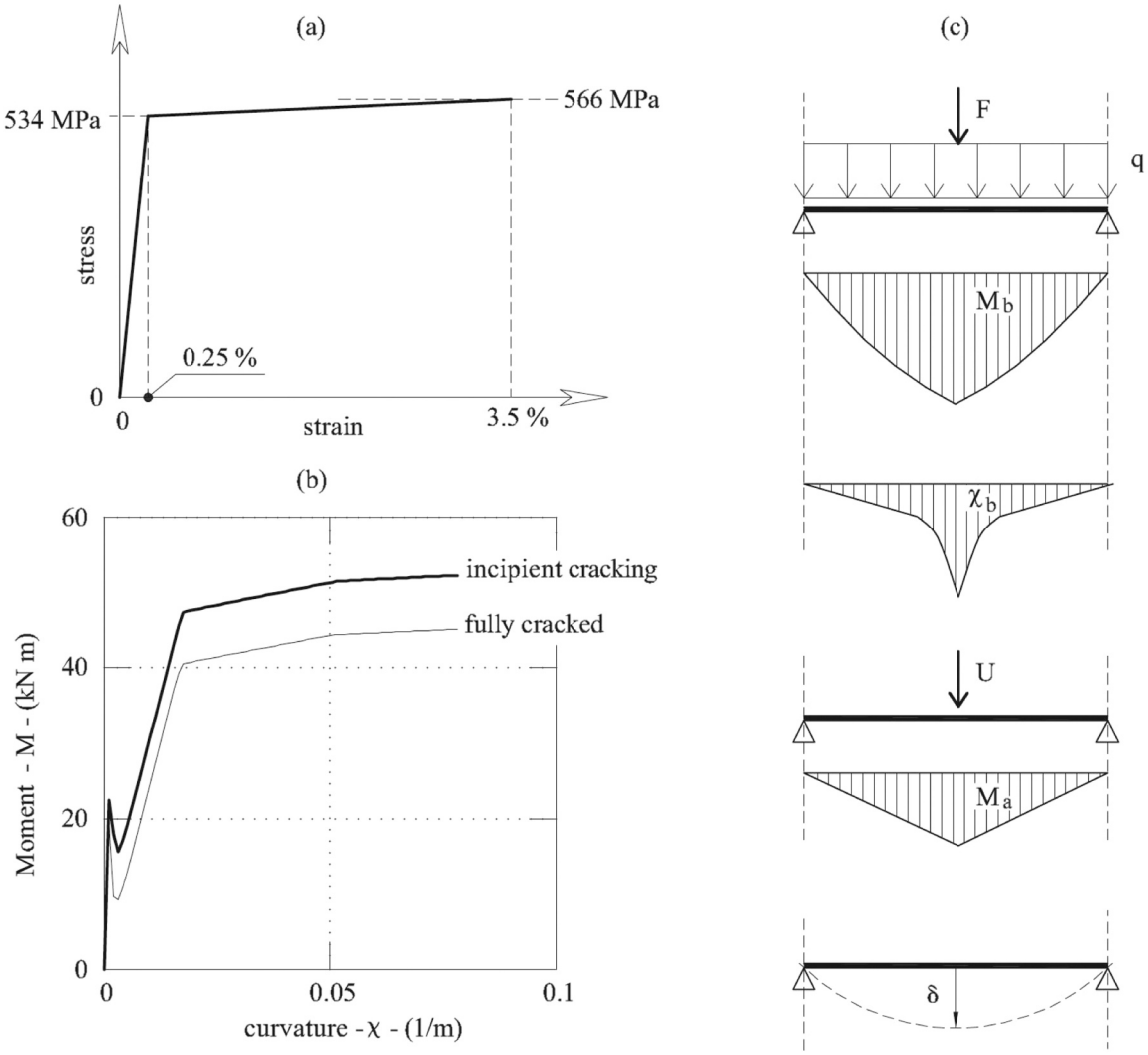

Fig. 10. Predicting the F-δ curves of the slabs with the three-stage model: (a) stress-strain relationship of steel rebar; (b) moment-curvature relationships of the slab cross-section; (c) real and virtual distributions of the bending moment and curvature.

Fig. 10b. In both the curves, the maximum curvature is reached when the compressive stress on the top edge of the I-shaped cross-section (Fig. 4a) is equal the compressive strength of the cast-in-situ concrete.

5.3. Stage 3 – Prediction of the slab deflection

When the geometry of the statically determinate beam depicted in Fig. 4 is known, and the M-χ relationships of the cross-sections are computed, the deflection δ corresponding to an applied load F on the slab can be evaluated by (see Fig. 10c):

1. Calculating the bending moment M_b in the real structure. It is produced by the load F of the loading machine and by the self-weight of the beam q.
2. Calculating the distributions of the curvature χ_b (corresponding to M_b) by means of the two moment-curvature relationships.
3. Defining a virtual system, made by the same beam and by a virtual load U (dual of the unknown deflection δ), and computing the virtual bending moment M_a.
4. Calculating the deflection δ with the following equation of virtual works:

$$\delta = \frac{1}{U}\int_0^{L_1} M_a \bullet \chi_b \quad dL \tag{4}$$

where L_1 is the length of the span (distance between the supports in Fig. 4b).

If these steps are repeated for all the loads F, a range of possible F-δ can be obtained.

As shown by the dashed curves in Fig. 11, this range is bordered by two the load-deflection curves F-δ, called Min T.S. and Max T.S., coming from the M-χ diagrams of incipient cracking and fully cracked cross-section, respectively.

5.4. Comparing the experimental F-δ curves with the range numerically computed

Fig. 11a shows the comparison between the range computed with the three-stage model and the F-δ curves measured in the tests on slab 1 and slab 2, having the same content of rebar. The different tension stiffening contribution in the two slabs (F-δ of slab 1 is closer to Min T.S curve, whereas F-δ of slab 2 is closer to Max T.S curve) can be ascribed to the concrete of predalles. The presence of fibers in concrete type A of slab 2 made it stiffer and stronger than slab 1, whose predalle did not contain any fiber. Indeed, fibers can produce a bridging effect and maintain the tensile strength in the precast part of the slab even in presence of large cracks, and after the yielding of the rebar. Therefore, the presence of a fiber-reinforcement compensated the loss of strength that occurred in concrete type A when a large part of CEM I 52.5 R (of concrete Ref.) was substituted by SCM (of CEM III 42.5). In other words, the application of the three-stage model furtherly confirms that when recycled materials are suitably used, the strength of full-scale structures can improve.

In the concrete type B of slab 3, the presence of RCA, in addition to SCM and RSF, increased the value of R without changing the F-δ curve of slab 1 (see Fig. 11b). Due to the fiber-reinforcement, the flexural stiffness of the slabs was sufficiently high to maintain the F-δ curve close to that of Max T.S. in service, whereas at ultimate limit state the curve of Min T.S. is more representative of the experimental results. This is also true for slab 4 (Fig. 11c), where rubber substituted the stone aggregate

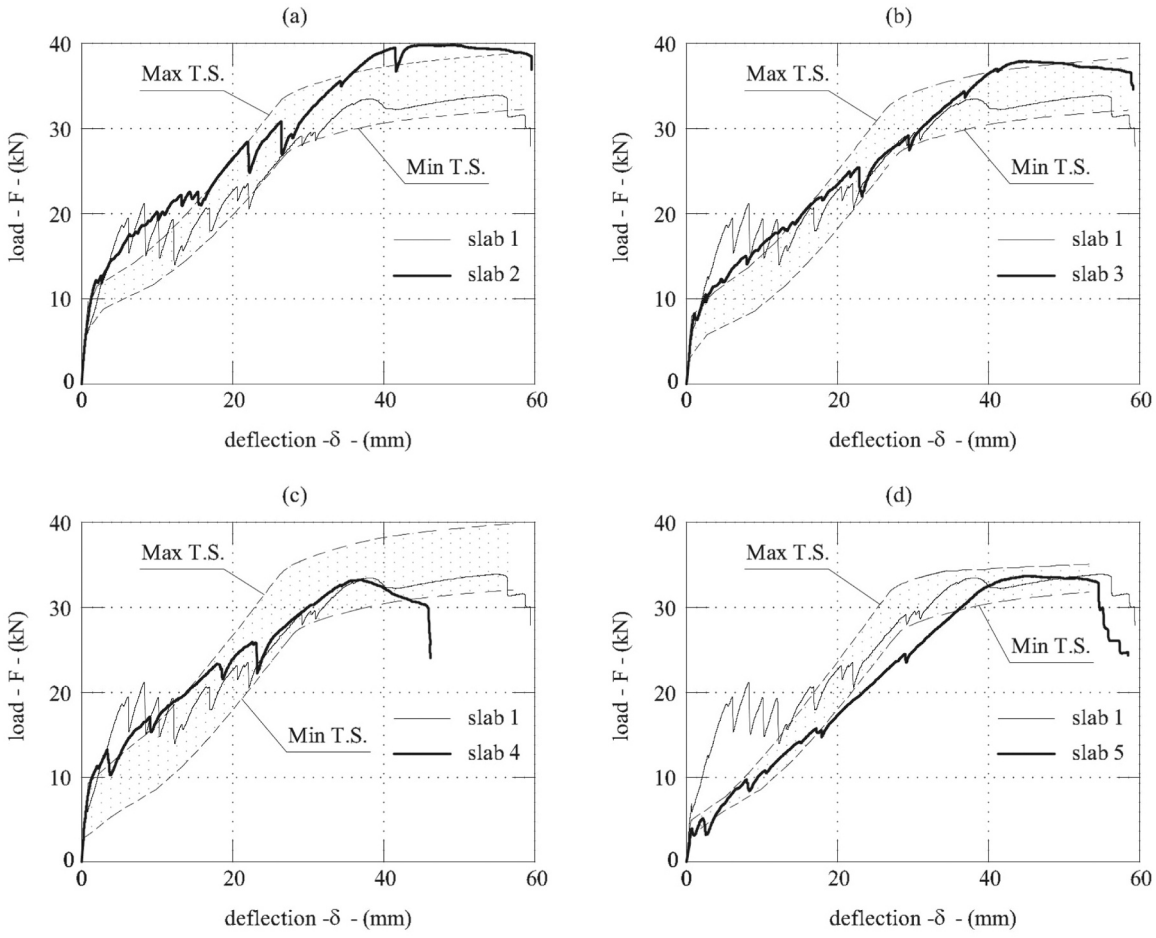

Fig. 11. Comparing the load-deflection F-δ response of the slabs experimentally measured, and the ranges theoretically predicted with the three-stage model.

of the predalle with RSF.

When both rubber and RCA substituted the virgin aggregate (i.e., in the predalle of slab 5), the reduction of tension stiffening with respect to slab 1 is more evident (Fig. 11d). Indeed, the width of the range computed with the three-stage model is narrower than in all the other cases. Moreover, the *F*-δ curve lies on the Min T.S. curve, except for 20 mm < δ < 38 mm, where it overestimates the load *P*. This is probably due to the sharp transition from the elastic regime to the strain hardening stage of the bilinear stress-strain law of steel (Fig. 10a), which increased the load *P* predicted by the model when the slope of the Min T.S. curve changes.

6. Conclusions

From the experimental campaign and the theoretical analyses described in the previous sections, aimed at applying the GPP in concrete slabs, the following conclusions can be drawn:

- By using RCA, rubber, and SCM, GPP are satisfied even if a reduction of compressive strength can be observed. Vice-versa, the loss of flexural strength can be compensated by using RSF.
- As in the case of the slab 2 tested in this research project, when recycled materials are suitably combined with the components of the concrete mixture of a predalle, the mechanical performances of the partially precast slabs are even better than those made with only virgin materials (i.e., slab 1).
- Through an eco-mechanical analysis, it is possible to select concrete, predalles, and full-scale slabs that satisfy GGP (i.e., the use of structural concrete with more than a pre-established percentage of recycled material) and the required mechanical performances.
- If concrete type B (with a percentage of recycled materials of 40%) is used in the predalles of partially prefabricated slabs, GPP can be satisfied in the whole load-bearing structure of a building, also when the cast-in-situ concrete is made with only virgin components. However, the use of type B concrete is currently impeded by building codes, which prescribe a minimum compressive strength also when this concrete is only used in the tensile zones of slabs in bending.
- The load-deflection responses of full-scale slabs made with predalles can be predicted with a three-stage model. In particular, by using the equivalence between fiber-reinforcement and traditional rebar, a range of possible load deflection diagrams can be calculated also when the concrete mixtures of predalles contain RSF and other recycled materials. In most of the cases, the response of the slabs experimentally measured falls within the range computed by the proposed model.

As the three-stage model based on the equivalent rebar is a sort of link between the prescriptions of GPP and structural performance, further tests will be performed with the aim of generalizing the application to other structures in bending, such as pavements.

CRediT authorship contribution statement

Fantilli Alessandro P.: Conceptualization, Data curation, Formal analysis, Funding acquisition, Investigation, Methodology, Project administration, Resources, Software, Supervision, Validation, Visualization, Writing – original draft, Writing – review & editing.

Declaration of Competing Interest

The authors declare that they have no known competing financial interests or personal relationships that could have appeared to influence the work reported in this paper.

Data Availability

Data will be made available on request.

Acknowledgment

The author wants to thank Botta Prefabbricati s.r.l. and ETRA for the technical support given to perform the experimental program described in this paper.

References

[1] Monteiro P, Miller S, Horvath A. Towards sustainable concrete. Nat Mater 2017;16:698–9. https://doi.org/10.1038/nmat4930.
[2] Mehta PK, Monteiro PJM. Concrete: Microstructure, Properties, and Materials. 4th ed. McGraw Hill Education; 2013.
[3] Bendixen M, Best J, Hackney C, Lønsmann Iversen L. Time is running out for sand. Nature 2019;571:29–31. https://doi.org/10.1038/d41586-019-02042-4.
[4] Habert G, Roussel N. Study of two concrete mix-design strategies to reach carbon mitigation objectives. Cem Concr Compos 2009;31(6):397–402. https://doi.org/10.1016/j.cemconcomp.2009.04.001.
[5] Lothenbach B, Scrivener K, Hooton RD. Supplementary cementitious materials. Cem Concr Res 2011;41(12):1244–56. https://doi.org/10.1016/j.cemconres.2010.12.001.
[6] Tam VWY, Soomro M, Evangelista ACJ. A review of recycled aggregate in concrete applications (2000–2017). Constr Build Mater 2018;172:272–92. https://doi.org/10.1016/j.conbuildmat.2018.03.240.
[7] Assaggaf RA, Ali MR, Al-Dulaijan SU, Maslehuddin M. Properties of concrete with untreated and treated crumb rubber – a review. J Mater Res Technol 2021;11:1753–98. https://doi.org/10.1016/j.jmrt.2021.02.019.
[8] Youssf O, El Gawady MA, Mills JE, Ma X. Analytical modeling of the main characteristics of crumb rubber concrete. Acids Spec Publ 2017;314:1–18. https://doi.org/10.14359/51689742.
[9] Hassanli R, Youssf O, Vincent T, Mills JE, Manalo A, Gravina RJ. Experimental study on compressive behavior of FRP-confined expansive rubberized concrete. J Compos Constr 2020;24(4):1–14. https://doi.org/10.1061/(ASCE)CC.1943-5614.0001038.
[10] Yi O, Zhuge Y, Ma X, Gravina RJ, Mills JE, Youssf O. Push-off and pull-out bond behaviour of CRC composite slabs – an experimental investigation. Eng Struct 2021;228:1–19. https://doi.org/10.1016/j.engstruct.2020.111480.
[11] Onuaguluchi O, Banthia N. Value-added reuse of scrap tire polymeric fibers in cement-based structural applications. J Clean Prod 2019;231:543–55. https://doi.org/10.1016/j.jclepro.2019.05.225.
[12] Qin X, Kaewunruen S. Environment-friendly recycled steel fibre reinforced concrete. Constr Build Mater 2022;327:126967. https://doi.org/10.1016/j.conbuildmat.2022.126967.
[13] European Commission (2016) Buying Green! A handbook on green public procurement. 3rd Edition https://ec.europa.eu/environment/gpp/buying_handbook_en.htm.
[14] Italian Ministry of Environment and Energy Security (2022) Minimal environmental criteria for the procurement of planning and services for new buildings, refurbishments and maintenance of buildings and the management of public administration construction sites. DM 256, 23/06/2022. https://gpp.mite.gov.it/sites/default/files/2022–08/GURI_183_06_08_22_Allegato_Edilizia.pdf.
[15] Bigaj-van Vliet A, Dieteren G, Matthews S. *fib* MC2020 - A Sustainability-Driven Performance-Based Approach to Design, Execution and Life-Cycle Management of Concrete Structures. In: Ilki A, Çavunt D, Çavunt YS, editors. Building for the Future: Durable, Sustainable, Resilient. fib Symposium 2023. Lecture Notes in Civil Engineering, vol 349. Cham: Springer; 2023. https://doi.org/10.1007/978-3-031-32519-9_7.
[16] Fennell P, Driver J, Bataille C, Davis SJ. Cement and steel — nine steps to net zero. Nature 2022;603:574–7. https://doi.org/10.1038/d41586-022-00758-4.
[17] PCI Concrete Handbook Committee (2017) PCI Design Handbook - Precast and Prestressed Concrete. Pre-cast/Prestressed Concrete Institute. 8th Edition.
[18] Chiaia B, Fantilli AP, Vallini P. Combining fiber-reinforced concrete with traditional reinforcement in tunnel linings. Eng Struct 2009;31(7):1600–6. https://doi.org/10.1016/j.engstruct.2009.02.037.
[19] Fantilli AP, Dehkordi FM. Two-stage cementitious composites containing recycled steel fibers. Acids Mater J 2022;119(2):197–206. https://doi.org/10.14359/51734300.
[20] FIB (2013) fib Model Code for Concrete Structures 2010. Ernst & Sohn. 1st Edition.
[21] UNI EN 14651 (2005) Test method for metallic fibered concrete - Measuring the flexural tensile strength (limit of proportionality (LOP), residual). European Committee for Standardization, Brussels.
[22] Fantilli AP. The Use of Recycled Steel Fibre in Precast Structures. In: Ilki A, Çavunt D, Çavunt YS, editors. Building for the Future: Durable, Sustainable, Resilient. fib Symposium 2023. Lecture Notes in Civil Engineering, vol 349. Cham: Springer; 2023. https://doi.org/10.1007/978-3-031-32519-9_109.
[23] Naaman AE. Strain hardening and deflection hardening fiber reinforced cement composites. In: Naaman AE, Reinhardt HW, editors. Proceedings of the 4th International RILEM Workshop on High Performance Fiber Reinforced Cement Composites. MI, USA: Ann Arbor; 2003. p. 95–113.

[24] ACI Committee 314 (2016) Guide to Simplified Design for Reinforced Concrete Buildings. ACI PRC-314–16.
[25] Fantilli AP, Nishiwaki T. Ecological and mechanical performances of ultra-high-performance fiber-reinforced cementitious composite containing fly ash. Acids Mater J 2023;120(1):5–16. https://doi.org/10.14359/51737330.
[26] Federbeton (2021) Sustainability report. https://www.federbeton.it/Portals/0/pubdoc/pubblicazioni/Rapporti/Rapporto_di_Sostenibilità_Federbeton_2021.pdf?ver=2022–10-10–123207-383 (in Italian).
[27] UNI EN 1992–1-1 (2004) Eurocode 2: Design of concrete structures - Part 1–1: General rules and rules for buildings. European Committee for Standardization, Brussels.
[28] Mujdeci A, Bompa D, Elghazouli A. Structural performance of composite steel rubberised concrete members under combined loading conditions. ce/Pap - Proc Civ Eng 2021;4:641–7. https://doi.org/10.1002/cepa.1343.
[29] Chopra AK. Dynamics of Structures: Theory and Applications to Earthquake Engineering. 5th ed. Pearson,; 2017.
[30] Fantilli AP, Orfeo B, Pérez Caldentey A. The deflection of reinforced concrete beams containing recycled steel fibers. Struct Concr 2021;22:2089–104. https://doi.org/10.1002/suco.202000729.
[31] Falkner H, Henke V. Steel fibre reinforced concrete, from research to standards. Concr Struct Annu Tech J Hung Group Fib 2005;6:39.

Update

Engineering Structures

Volume 303, Issue , 15 March 2024, Page

DOI: https://doi.org/10.1016/j.engstruct.2024.117536

Engineering Structures 303 (2024) 117536

Contents lists available at ScienceDirect

Engineering Structures

journal homepage: www.elsevier.com/locate/engstruct

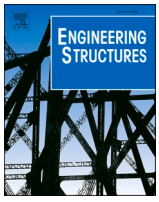

Corrigendum

Corrigendum to 'Green Public Procurement Applied to Partially Precast Reinforced Concete Slabs', [Engineering Structures, 301 (2024) 117338]

Alessandro P. Fantilli

Dept. of Structural, Building and Geotechnical Engineering - DISEG, Politecnico di Torino, Corso Duca degli Abruzzi 24, Torino 10129, Italy

The authors regret to inform you that there is mistake in the title of this paper, where "CONCETE" was written in place of "CONCRETE".

The authors would like to apologise for any inconvenience caused.

DOI of original article: https://doi.org/10.1016/j.engstruct.2023.117338.

E-mail address: alessandro.fantilli@polito.it.

https://doi.org/10.1016/j.engstruct.2024.117536

Available online 20 January 2024